



**HAL**  
open science

## Sound Velocities and Elastic Moduli of Phases I and V of Silicon at High Pressures

Bin Zhao, Feng Xu, Laurent Belliard, Haijun Huang, Bernard Perrin, Philippe Djemia, Andreas Zerr

► **To cite this version:**

Bin Zhao, Feng Xu, Laurent Belliard, Haijun Huang, Bernard Perrin, et al.. Sound Velocities and Elastic Moduli of Phases I and V of Silicon at High Pressures. *physica status solidi (RRL) - Rapid Research Letters*, 2019, 13 (8), pp.1900173. 10.1002/pssr.201900173 . hal-02316887

**HAL Id: hal-02316887**

**<https://hal.science/hal-02316887v1>**

Submitted on 7 Nov 2023

**HAL** is a multi-disciplinary open access archive for the deposit and dissemination of scientific research documents, whether they are published or not. The documents may come from teaching and research institutions in France or abroad, or from public or private research centers.

L'archive ouverte pluridisciplinaire **HAL**, est destinée au dépôt et à la diffusion de documents scientifiques de niveau recherche, publiés ou non, émanant des établissements d'enseignement et de recherche français ou étrangers, des laboratoires publics ou privés.

## Sound velocities and elastic moduli of phases I and V of silicon at high pressures

*Bin Zhao, Feng Xu\*, Laurent Belliard, Haijun Huang, Bernard Perrin, Philippe Djemia and Andreas Zerr\**

B. Zhao, Dr. F. Xu, Prof. H. Huang  
School of Science, Wuhan University of Technology, 430070 Wuhan, China  
E-mail: (xufeng@whut.edu.cn)

Prof. L. Belliard, Dr. B. Perrin  
Sorbonne Université, UPMC Université Paris 06, CNRS UMR 7588,  
Institut des NanoSciences de Paris (INSP), 75005 Paris, France

Prof. P. Djemia, Dr. A. Zerr  
Laboratoire des Sciences des Procédés et des Matériaux (LSPM), UPR-CNRS 3407,  
Université Paris Nord, 93430 Villetaneuse, France  
E-mail: (zerr@univ-paris13.fr)

Keywords: (silicon, high-pressure phases, sound velocities, elastic moduli)

### Abstract

Pressure dependences of longitudinal sound velocities, in the two phases Si-I and Si-V of silicon having, respectively, cubic-diamond and primitive-hexagonal structures, are measured using the technique of picosecond laser ultrasonics adapted to samples compressed in a diamond anvil cell (DAC). For the Si-I phase, stable at atmospheric pressure, the longitudinal sound velocity along the  $\langle 100 \rangle$  direction is obtained in a single crystal up to 9 GPa. In the case of the Si-V phase, the average sound velocity for an isotropic polycrystalline sample  $V_{L(\text{avg})}$  is measured for the first time between 18 and 27 GPa. Above this pressure, preferred orientation of the hexagonal crystallites of Si-V with their  $c$ -axes parallel to the compressional direction in the DAC, and to the acoustic pulse propagation direction, is progressively developing thus precluding further  $V_{L(\text{avg})}$  measurement. The experimental single

1 crystal elastic constants  $C_{11}(P)$  and  $C_{12}(P)$  of Si-I, and the shear modulus of  
2 polycrystalline Si-V deduced here are in a very good agreement with our first  
3 principles calculations and with the earlier results reported for Si-I.  
4  
5  
6  
7

## 8 **Main text**

9  
10 Silicon has come into wide use in semiconductor field and become the basic material  
11 due to its chemical, physical and technical properties at atmospheric pressure. Upon  
12 compression, silicon metalizes and undergoes a series of phase transitions, and thus is  
13 considered as an example elemental solid in pressure-induced phase transition studies.  
14  
15  
16  
17  
18  
19  
20  
21

22 Crystal structures, phase stability, related lattice dynamic properties were the subjects  
23 of intense experimental and theoretical interest over the past decades.<sup>[1,2,3]</sup> X-ray  
24 diffraction studies indicated that the sequential structural transitions of silicon with  
25 increasing pressure are as follows: cubic-diamond (Si-I)  $\rightarrow$   $\beta$ -Sn (Si-II)<sup>[4]</sup>  $\rightarrow$  *Imma*  
26 (Si-XI)<sup>[5]</sup>  $\rightarrow$  primitive-hexagonal (Si-V)<sup>[6]</sup>  $\rightarrow$  *Cmca* (Si-VI)<sup>[6]</sup>  $\rightarrow$  hexagonal  
27 closed-packed (Si-VII)<sup>[6]</sup>  $\rightarrow$  face-centered cubic (Si-X, up to 248 GPa)<sup>[7]</sup>. Si-II, Si-XI  
28 and Si-VI phases are stable in quite narrow pressure regions,<sup>[8]</sup> and exist as single  
29 phases in even narrower regions due to coexistence with the adjacent phases. In  
30 contrast, Si-I, Si-V, Si-VII and Si-X exist as single phases in extended pressure ranges.  
31  
32  
33  
34  
35  
36  
37  
38  
39  
40  
41  
42  
43  
44  
45  
46  
47  
48  
49  
50  
51  
52  
53  
54  
55  
56  
57  
58  
59  
60  
61  
62  
63  
64  
65

1 was reported yet.

2  
3 Knowledge of sound velocities of solids at high pressures allows a better  
4  
5 understanding of their intrinsic elastic properties, especially of  $G(P)$ , which is very  
6  
7 sensitive to subtle phase transitions,<sup>[13]</sup> defects or inhomogeneities,<sup>[14]</sup> and permits a  
8  
9 contrast-rich 3D tomography of non-uniform bodies.<sup>[15]</sup> However, measurement of  
10  
11 sound velocities at high pressures is challenging, even using standard ultrasonic  
12  
13 techniques or more recent synchrotron-based scattering techniques.<sup>[16]</sup> In contrast to  
14  
15 standard ultrasonic techniques applicable in a limited pressure range, inelastic X-ray  
16  
17 scattering permits measurement of longitudinal sound velocity  $V_L$  for a sample  
18  
19 compressed in a DAC to very high pressures. However, it requires use of synchrotron  
20  
21 radiation, large set-ups, very long counting times, and is only suited for samples  
22  
23 containing elements with  $Z$  between 30 and 50.<sup>[16]</sup> The related technique of nuclear  
24  
25 resonant inelastic X-ray scattering requires samples containing Mössbauer isotopes  
26  
27 and theoretical modeling in order to extract sound velocities from the recorded signals.  
28  
29 Thus, none of the last two techniques is suitable for the acoustic measurements on  
30  
31 silicon samples in a DAC. At pressures above  $\sim 20$  GPa, combination of DAC with  
32  
33 picosecond laser ultrasonics (PLU) provides access to sound velocities of opaque  
34  
35 solids such as silicon.<sup>[17,18]</sup> Recently, the PLU based on phonon imaging was  
36  
37 demonstrated to permit extraction of a complete set of  $C_{ij}$  of Si-I compressed in a  
38  
39 DAC.<sup>[12]</sup> However, this method is less accurate when loading conditions become  
40  
41 non-hydrostatic and deformations of the sample surface seriously influence the  
42  
43 interferometric detection of the phonon imaging. Moreover, the acoustic mapping  
44  
45  
46  
47  
48  
49  
50  
51  
52  
53  
54  
55  
56  
57  
58  
59  
60

1 analysis requires single crystals which are difficult to preserve at ultrahigh pressures  
2  
3 and upon phase transitions.  
4

5  
6 The pump-probe technique called time-domain Brillouin scattering (TDBS) <sup>[19]</sup> could  
7  
8 be potentially applied to measure  $V_L(P)$  of semiconducting Si-I, below ~9 GPa, due to  
9  
10 a relatively long optical penetration depth of the laser radiation with the wavelength  
11  
12  $\lambda=800$  nm. However, no Brillouin oscillations with frequencies above ~78 GHz,  
13  
14 expected for Si at 1 atm. or higher pressures, were observed in our trial TDBS  
15  
16 experiments. For this reason, the PLU based on the pulse-echo method was applied to  
17  
18 measure  $V_L$  of both Si-I and Si-V. Ultrafast acoustic pulses were generated and their  
19  
20 arrivals detected by a conventional PLU setup equipped with a stabilized Michelson  
21  
22 interferometer.<sup>[20]</sup> Briefly, a mode-locked Ti:sapphire laser (MAI-TAI Spectra,  $\lambda=800$   
23  
24 nm) operating with a repetition rate of 80 MHz and a pulse width of <100 fs was split  
25  
26 into a pump and a probe beam. The photon frequency of the pump beam was doubled  
27  
28 to ensure an efficient generation of acoustic pulses in silicon.<sup>[21]</sup> The beams were then  
29  
30 focused on opposite sides of a sample with  $\times 50$  microscope objectives to spots of ~2  
31  
32  $\mu\text{m}$  in diameter (**Figure 1**). The probe beam measured the transient reflectivity change  
33  
34 of the sample surface, induced by arriving acoustic pulses, as a function of the time  
35  
36 delay between the pump and probe beams. Three samples were studied in this work.  
37  
38 These were single crystals of silicon having thicknesses of  $h_0=9.74$   $\mu\text{m}$  (subscript 0  
39  
40 indicates values at 1 atm.) which surfaces were oriented along (001) and covered with  
41  
42 thin metallic films on one or both sides to enhance the photon-acoustic transduction  
43  
44 efficiency. In present work, the FeSi<sub>0.2</sub> alloy and Ti were employed. Titanium is  
45  
46  
47  
48  
49  
50  
51  
52  
53  
54  
55  
56  
57  
58  
59  
60

1 extensively used as a transducer in PLU because it exhibits strong photo-elastic  
2  
3 coefficients in the near infrared range, when the photon energy is close to an interband  
4  
5 transition.<sup>[22]</sup> However, delamination precludes deposition of thick Ti-films ( $>0.5 \mu\text{m}$ )  
6  
7  
8 needed for a reliable detection of acoustic pulse arrivals, especially at high pressures  
9  
10 when the  $V_L$  increases and the film thickness decreases. In the first trial experiments  
11  
12 (run 1) where both sample sides were covered with the metallic films,  
13  
14 Ti(350nm)/Si/FeSi<sub>0.2</sub>(500nm), we have found that FeSi<sub>0.2</sub> is well suited for acoustic  
15  
16 pulse detection. Moreover, thick FeSi<sub>0.2</sub> films could be deposited on Si without  
17  
18 delamination. Because acoustic pulses could be generated directly and efficiently on  
19  
20 Si using the pump beam with  $\lambda=400 \text{ nm}$ ,<sup>[21]</sup> samples covered with FeSi<sub>0.2</sub> films on one  
21  
22 side, FeSi<sub>0.2</sub>(1 $\mu\text{m}$ )/Si, were used in the runs 2 and 3. The samples were compressed in  
23  
24 a DAC with beveled diamond anvils having culets of 300  $\mu\text{m}$  in diameter. A hole of  
25  
26  $\sim 100 \mu\text{m}$  in diameter, drilled in a steel gasket pre-indented to the thickness of  $\sim 40 \mu\text{m}$ ,  
27  
28 served as the sample volume. The samples were placed on one of the anvils and the  
29  
30 remaining volume was filled with NaCl which served as a pressure transmitting  
31  
32 medium (PTM) (Figure 1). Fluorescence of small ruby grains placed near the sample  
33  
34 was used to measure pressure.<sup>[23]</sup>

35  
36  
37 All first-principles calculations in this work were based on the density functional  
38  
39 theory (DFT) as implemented in the Vienna Ab-initio Simulation Package  
40  
41 (VASP).<sup>[24,25]</sup> The total energy per atom was evaluated with  $10^{-3} \text{ meV/atom}$   
42  
43 convergence accuracy, for both cubic (space group  $Fd\bar{3}mO1$ ) and hexagonal (space  
44  
45 group  $P63/mmc$ ) cells containing four and two atoms, respectively. The electron-ion  
46  
47  
48  
49  
50  
51  
52  
53  
54  
55  
56  
57  
58  
59  
60

1 interactions were described by the projector augmented wave method (PAW)<sup>[26]</sup> with a  
2  
3 plane wave energy cutoff of 800 eV for cell optimizations, under the generalized  
4  
5 gradient approximation (GGA) with a Perdew-Burke-Ernzerhof (PBE) exchange  
6  
7 correlation functional.<sup>[27]</sup> The Monkhorst-Pack scheme<sup>[28]</sup> was used to construct  
8  
9  $k$ -meshes with  $0.5 \text{ nm}^{-1}$  spacing for self-consistent calculations.  
10  
11

12  
13  
14 An example of measured transient reflectivity used to extract  $V_L$  for one of our  
15  
16 samples is shown in Figure 1. From such a record, the  $V_L$  value was determined using  
17  
18 the relation:  $V_L=2h/\Delta t$ , where  $\Delta t$  is duration of the acoustic pulse roundtrip in the  
19  
20 silicon sample having thickness  $h$ . The latter was great enough to guarantee an  
21  
22 excellent accuracy for the  $\Delta t$  determination ( $<5 \text{ ps}$ ) which corresponds to the  $V_L$   
23  
24 uncertainty below 0.2%. The sample thickness on compression was deduced from the  
25  
26 measured here lateral area of the sample surface  $S$  and the earlier reported equation of  
27  
28 state (EOS),  $V(P)$ .<sup>[2]</sup> At each pressure step, we recorded an optical image of the  
29  
30 sample and used it to determine pressure dependence of the ratio  $S(P)/S_0$ . Dividing the  
31  
32 known  $V(P)/V_0$  for all silicon phases by our  $S(P)/S_0$ , we obtained the relative thickness  
33  
34 change  $h(P)/h_0$ . In the case of Si-I, the obtained dependence obeyed the earlier  
35  
36 measured EOS:  $h(P)/h_0=[V(P)/V_0]^{1/3}$  which indicated that the loading conditions were  
37  
38 close to hydrostatic and that the sample remained a single crystal till 9 GPa, close to  
39  
40 the onset of the transition to Si-II. Above this transition, the correlation between  
41  
42  $h(P)/h_0$  and  $V(P)/V_0$  did not hold anymore thus suggesting plastic deformation of the  
43  
44 sample due to growing non-hydrostaticity upon compression and low hardnesses of  
45  
46 the high-pressure metallic phases of silicon. For this reason, thickness of the samples  
47  
48  
49  
50  
51  
52  
53  
54  
55  
56  
57  
58  
59  
60

1 at  $P > 10$  GPa was determined using the expression:  $h(P) = h_0 [V(P)/V_0] [S_0/S(P)]$ . We  
2  
3 note that the  $S(P)$  and, accordingly,  $h(P)$  above 10 GPa was determined with the  
4  
5 uncertainty of less than  $\sim 2.5\%$ , much larger than that of  $\Delta t$ .  
6  
7

8  
9 Our experimental  $V_L$  values for all three runs are shown in **Figure 2**. Because Si-II  
10  
11 and Si-XI coexist with the neighbor phases, and their volume ratios have not been  
12  
13 well established in the literature, further analysis of the dependences  $V_L(P)$  between 9  
14  
15 and 18 GPa was not meaningful. At pressures where only Si-I is present, up to 9 GPa,  
16  
17 the measured  $V_L(P)$  corresponds to that along  $\langle 100 \rangle$ . This is supported by the  
18  
19 comparison with the value  $V_{L\langle 100 \rangle}(P)$  we calculated for the same direction in a single  
20  
21 crystal of Si-I (Figure 2). Combining our  $V_{L\langle 100 \rangle}(P)$  and the EOS,<sup>[2]</sup> providing mass  
22  
23 density  $\rho(P)$  and bulk modulus  $B(P)$ , we derived pressure dependences of  $C_{11}(P)$  and  
24  
25  $C_{12}(P)$  using the well-known expressions:  $C_{11} = \rho V_{L\langle 100 \rangle}^2$  and  $C_{12} = (3B -$   
26  
27  $C_{11})/2$ . In **Figure 3** we compare our experimental and theoretical  $C_{11}(P)$  and  $C_{12}(P)$   
28  
29 with the earlier experimental and theoretical results.<sup>[10,11,12]</sup> An overall good  
30  
31 agreement is found, even though our GGA values are  $\sim 10\%$  lower than those  
32  
33 calculated within the local density approximation (LDA).  
34  
35

36  
37 At pressures where only Si-V exists, between 18 GPa and 38 GPa, our measured  $V_L(P)$   
38  
39 increases slowly with compression up to  $\sim 27$  GPa. This dependence agrees with the  
40  
41  $V_{L(\text{avg})}(P)$  we calculated for a polycrystalline sample of Si-V with randomly oriented  
42  
43 grains. The value of  $V_{L(\text{avg})}(P)$  is given by the expression:  $V_{L(\text{avg})} = \sqrt{(3B + 4G)/3\rho}$   
44  
45 where the isotropic moduli  $B(P)$  and  $G(P)$  were derived from our calculated  $C_{ij}(P)$  and  
46  
47  $\rho(P)$  using the Voigt-Reuss-Hill approximation. This observation indicated that up to  
48  
49  
50  
51  
52  
53  
54  
55  
56  
57  
58  
59  
60



1 ~27 GPa the sample of Si-V was texture free. Applying the inverse equation  $G =$   
2  
3  $3[\rho V_{L(avg)}^2 - B]/4$  to our experimental data-points and the earlier measured  $\rho(P)$   
4  
5 and  $B(P)$ , the experimental dependence  $G(P)$  for a polycrystalline texture-free sample  
6  
7 of Si-V was derived to 27 GPa (Figure 3).  
8  
9

10 It can be recognized in Figure 2 that above ~27 GPa our experimental  $V_L(P)$  increases  
11  
12 much faster with pressure than below and strongly deviates from our theoretical  
13  
14  $V_{L(avg)}(P)$ . This suggests a significant texturing of the sample of Si-V upon  
15  
16 compression above 27 GPa. Because the measured  $V_L(P)$  approaches the maximal  
17  
18 possible value in a hexagonal single crystal of Si-V (known to be along the  $c$ -axis,  
19  
20  $V_{L(0001)}$ ), we may conclude that the developing texture was characterized by a growing  
21  
22 number of grains which  $c$ -axes oriented along the propagation direction of the sound  
23  
24 pulses, perpendicular to the anvil culets. This observation agrees with an earlier XRD  
25  
26 work where strong changes in the intensity of the (001) and (100) peaks of Si-V were  
27  
28 recognized at similar pressures.<sup>[7]</sup> We also show in Figure 2  $V_L(P)$  derived for the  
29  
30 mixed phase region using our  $S(P)/S_0$ , an earlier EOS and the same equation  
31  
32  $h(P)=h_0[V(P)/V_0][S_0/S(P)]$ . Here, we assumed that above ~10 GPa the sample  
33  
34 contained Si-II and the following Si-XI phases only. This explains the sudden  
35  
36 step-like decrease in  $V_L(P)$  which should not appear in the case of an extended two  
37  
38 phase region. These data were not further treated due to the absence of such  
39  
40 information and are presented here only for completeness.  
41  
42  
43  
44  
45  
46  
47  
48  
49  
50  
51  
52  
53  
54

55 In conclusion, we investigated experimentally and theoretically pressure dependences  
56  
57 of the longitudinal sound velocities and elastic moduli of Si-I and Si-V. Under  
58  
59  
60

1 compression, the starting single crystals of Si-I underwent phase transitions and  
2 polycrystalline phases with small randomly orientated grains appeared. After the three  
3 phase transitions, the samples of Si-V could be regarded as elastically isotropic. For  
4 the Si-I phase, the measured  $V_L(P)$  corresponds therefore to that along the  $\langle 100 \rangle$   
5 direction,  $V_{L\langle 100 \rangle}(P)$ . For Si-V, the measured  $V_L(P)$  corresponds to that of an isotropic  
6 polycrystalline body  $V_{L(\text{avg})}(P)$  but only below 27 GPa. The dependences  $C_{11}(P)$  and  
7  $C_{12}(P)$  of Si-I, we derived from the experimental  $V_{L\langle 100 \rangle}(P)$  using the earlier measured  
8 EOS, are in a very good agreement with previously published data and with our  
9 calculations. More important, we measured for the first time  $V_L(P)$  and  $G(P)$  for  
10 polycrystalline Si-V between 18 GPa and 27 GPa. Above 27 GPa, we observed  
11 texturing of the polycrystalline Si-V whose grains preferably oriented with their  
12  $c$ -axes along the compressional direction in the DAC.  
13  
14  
15  
16  
17  
18  
19  
20  
21  
22  
23  
24  
25  
26  
27  
28  
29  
30  
31  
32

### 33 **Acknowledgements**

34 The authors acknowledge financial support from NSFC (projects No.41504070 and  
35 No.41874103) and CSC (File No.201606955092). We would like to thank L. Becerra  
36 for sample preparation; E. Peronne for experimental assistance; Y. Wu and X. Liu for  
37 fruitful discussion. We acknowledge access to the cluster MAGI of University Paris  
38 13 and N. Greneche for this support.  
39  
40  
41  
42  
43

44 Received: ()

45 Revised: ()

46 Published online: ()  
47  
48  
49

### 50 **References**

- 51 [1] A. Mujica, A. Rubio, A. Munoz, R. J. Needs, *Rev. Mod. Phys.* **2003**, 75, 863.  
52  
53 [2] R. J. Needs, A. Mujica, *Phys. Rev. B* **1995**, 51, 9652.  
54  
55 [3] Y. He, L. Zhong, F. Fan, C. Wang, T. Zhu, S. X. Mao, *Nat. Nanotechnol.* **2016**, 11,  
56  
57  
58  
59  
60

1 866.

2  
3 [4] J. C. Jamieson, *Science* **1963**, 139, 762.

4  
5  
6 [5] M. I. McMahon, R. J. Nelmes, *Phys. Rev. B* **1993**, 47, 8337.

7  
8  
9 [6] H. Olijnyk, S. K. Sikka, W. B. Holzapfel, *Phys. Lett. A* **1984**, 103, 137.

10  
11 [7] S. J. Duclos, Y. K. Vohra, A. L. Ruoff, *Phys. Rev. B* **1990**, 41, 12021.

12  
13  
14 [8] M. I. McMahon, R. J. Nelmes, N. G. Wright, D. R. Allan, *Phys. Rev. B* **1994**, 50,  
15  
16  
17 739.

18  
19  
20 [9] M. Hanfland, U. Schwarz, K. Syassen, K. Takemura, *Phys. Rev. Lett.* **1999**, 82,  
21  
22  
23 1197.

24  
25 [10] H. J. McSkimin, P. Andereatch, *J. Appl. Phys.* **1964**, 35, 2161.

26  
27 [11] B. B. Karki, G. J. Ackland, J. Crain, *J. Phys.-Condens. Mat.* **1997**, 9, 8579.

28  
29 [12] F. Decremps, L. Belliard, M. Gauthier, B. Perrin, *Phys. Rev. B* **2010**, 82, 104119.

30  
31 [13] N. Cai, T. Chen, X. Qi, B. Li, , *J. Appl. Phys.* **2018**, 124, 185901.

32  
33  
34 [14] Y. Wang, D. H. Hurley, Z. Hua, G. Sha, S. Raetz, V. E. Gusev, M. Khafizov, *Scr.*  
35  
36  
37  
38  
39  
40  
41  
42  
43  
44  
45  
46  
47  
48  
49  
50  
51  
52  
53  
54  
55  
56  
57  
58  
59  
60  
61  
62  
63  
64  
65  
*Mater.* **2019**, 166, 34.

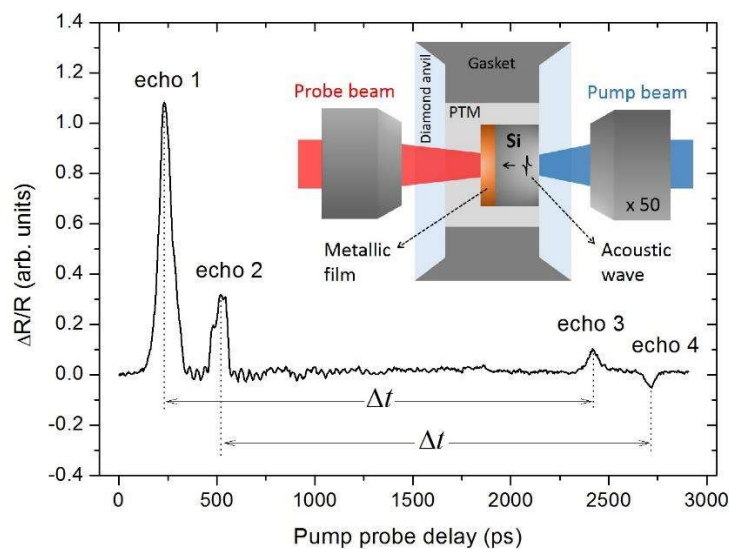
[15] P. Clouzet, Y. Masson, B. Romanowicz, *Geophys. J. Int.* **2018**, 213, 1849.

[16] R. J. Angel, J. M. Jackson, H. J. Reichmann, S. Speziale, *Eur. J. Mineral.* **2009**,  
21, 525.

[17] F. Decremps, L. Belliard, B. Perrin, M. Gauthier, *Phys. Rev. Lett.* **2008**, 100,  
035502.

[18] F. Decremps, M. Gauthier, S. Ayrinhac, L. Bove, L. Belliard, B. Perrin, M.  
Morand, G. Le Marchand, F. Bergame, J. Philippe, *Ultrasonics* **2015**, 56, 129.

- [19] S. M. Nikitin, N. Chigarev, V. Tournat, A. Bulou, D. Gasteau, B. Castagnede, A. Zerr, V. E. Gusev, *Sci. Rep.* **2015**, *5*, 9352.
- [20] F. Xu, L. Belliard, D. Fournier, E. Charron, J.-Y. Duquesne, S. Martin, C. Secouard, B. Perrin, *Thin Solid Films* **2013**, *548*, 366.
- [21] K. Ishioka, A. Rustagi, U. Hofer, H. Petek, C. J. Stanton, *Phys. Rev. B* **2017**, *95*, 035205.
- [22] A. Devos, A. Le Louarn, *Phys. Rev. B* **2003**, *68*, 045405.
- [23] H. K. Mao, J. Xu, P. M. Bell, *J. Geophys. Res. -Sol. Ea.* **1986**, *91*, 4673.
- [24] G. Kresse, J. Hafner, *Phys. Rev. B* **1993**, *47*, 558.
- [25] G. Kresse, J. Furthmüller, *Comput. Mater. Sci.* **1996**, *6*, 15-50.
- [26] G. Kresse, D. Joubert, *Phys. Rev. B* **1999**, *59*, 1758.
- [27] J.P. Perdew, K. Burke, M. Ernzerhof, *Phys. Rev. Lett.* **1996**, *77*, 3865.
- [28] H. J. Monkhorst, J. D. Pack, *Phys. Rev. B* **1976**, *13*, 5188.



1 **Figure 1.** Relative change of reflectivity of the sample surface as a function of  
2  
3 pump-probe delay recorded in the run 2 at  $P=6.3$  GPa. The acoustic pulse generated  
4  
5 on the silicon side propagated in the sample and reflected from different interfaces.  
6  
7 The echo 1 corresponds to the first arrival of the pulse on the opposite side. A part of  
8  
9 it, reflected at the interface  $\text{FeSi}_{0.2}$ (1 $\mu\text{m}$  thick film)/NaCl, returns as echo 2 after the  
10  
11 roundtrip in the  $\text{FeSi}_{0.2}$  film. The time intervals  $\Delta t$  between echoes 1 and 3 as well as  
12  
13 echoes 2 and 4 correspond to the pulse roundtrip in silicon. The polarity of different  
14  
15 echoes can be explained by acoustic reflectivity at the interfaces of the sample  
16  
17 materials with different acoustic impedances:<sup>[20]</sup> the lowest one for NaCl, followed by  
18  
19 Si and  $\text{FeSi}_{0.2}$ , and the highest for diamond. Brillouin oscillations,<sup>[19]</sup> visible after the  
20  
21 arrival of the echo 1, result from interferences of the probe beam reflected from  
22  
23 stationary surfaces and from the leaky acoustic pulse propagating in NaCl, used as the  
24  
25 PTM. Inset: schematic representation of the sample inside a DAC. The pump beam is  
26  
27 focused on the Si side while the probe beam on the  $\text{FeSi}_{0.2}$  side.  
28  
29  
30  
31  
32  
33  
34  
35  
36  
37  
38  
39  
40  
41  
42  
43  
44  
45  
46  
47  
48  
49  
50  
51  
52  
53  
54  
55  
56  
57  
58  
59  
60  
61  
62  
63  
64  
65

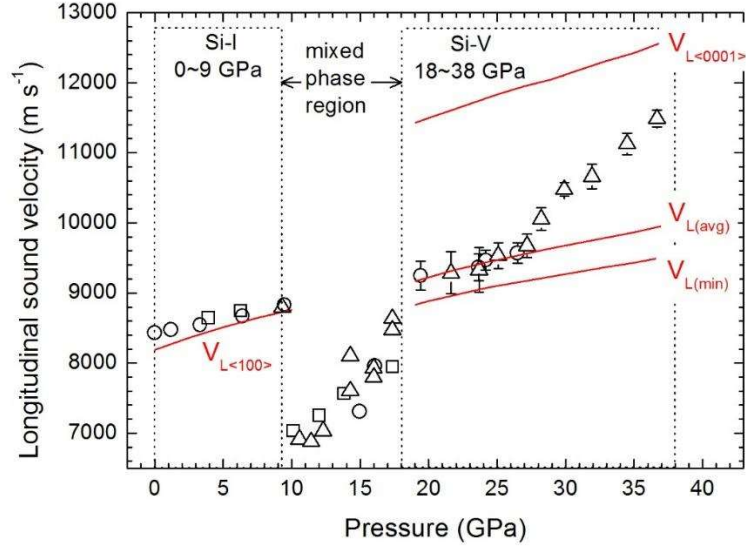


**Figure 2.** Longitudinal sound velocities of silicon as a function of pressure. The left and right framed ranges bracket pressures where only Si-I (0-9 GPa) and Si-V (18-38 GPa) exist. In the mixed phase region, the Si-I/Si-II, Si-II/Si-XI and Si-XI/Si-V may coexist (see text). The experimental data for the runs 1, 2 and 3 are shown by open circles, squares and triangles, respectively. For the pure Si-I region, the experimental uncertainties in  $V_L$  are smaller than the symbols. Results of our first-principles calculations are presented by solid red lines:  $V_{L\langle 100 \rangle}$  is the sound velocity along  $\langle 100 \rangle$  in Si-I,  $V_{L\langle \min \rangle}$  and  $V_{L\langle 0001 \rangle}$  are the minimal and maximal values in a hexagonal single crystal of Si-V where  $V_{L\langle 0001 \rangle}$  corresponds to the velocity along the  $c$ -axis,  $V_{L\langle \text{avg} \rangle}$  is that derived for polycrystalline Si-V using our theoretical  $C_{ij}(P)$ ,  $\rho(P)$  and the Voigt-Reuss-Hill approximation.

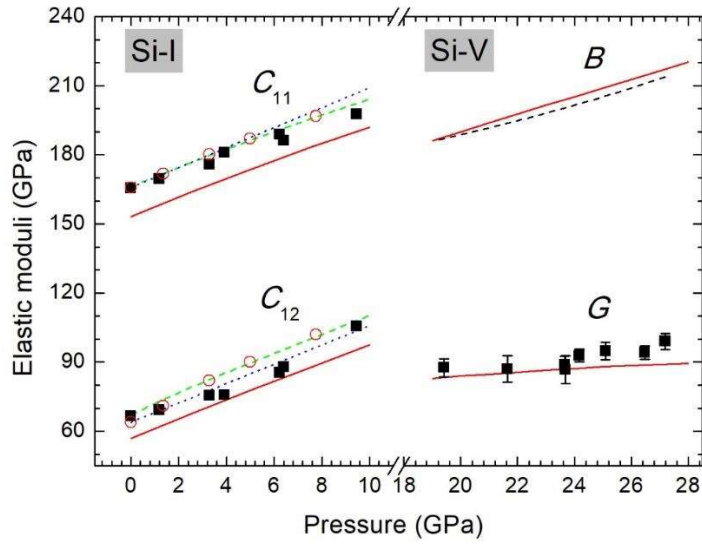


**Figure 3.** Pressure dependences of elastic moduli of the Si-I and Si-V phases.  $C_{11}$  and  $C_{12}$  indicate the corresponding single crystal elastic constants of Si-I. Our measured values (solid black squares) are compared with the earlier ones obtained by the phonon imaging method (open red circles)<sup>[12]</sup> and by a traditional ultrasonic technique (dotted blue lines).<sup>[10]</sup> Our *ab-initio* results within GGA (solid red lines) are compared with the earlier predictions within LDA (dashed green lines).<sup>[11]</sup> Above 18 GPa, the solid black squares represent  $G(P)$  of polycrystalline Si-V measured here and the dashed black line  $B(P)$ <sup>[2]</sup> measured earlier. Our theoretical  $B(P)$  and  $G(P)$  are represented by solid red lines.